



Contents lists available at ScienceDirect

Archives of Biochemistry and Biophysics

journal homepage: www.elsevier.com/locate/yabbi

Mechanistic studies of the tyrosinase-catalyzed oxidative cyclocondensation of 2-aminophenol to 2-aminophenoxazin-3-one



Courtney Washington^a, Jamere Maxwell^a, Joenathan Stevenson^a, Gregory Malone^a, Edward W. Lowe Jr.^b, Qiang Zhang^a, Guangdi Wang^a, Neil R. McIntyre^{a,*}

^a Division of Mathematical and Physical Sciences, Department of Chemistry, Xavier University of Louisiana, New Orleans, LA 70125, USA

^b Center for Structural Biology, Vanderbilt University, Nashville, TN 37232, USA

ARTICLE INFO

Article history:

Received 6 January 2015

and in revised form 20 April 2015

Available online 14 May 2015

Keywords:

Isotope effect

Tyrosinase

2-Aminophenol

Mechanism

Cyclocondensation

Kinetics

ABSTRACT

Tyrosinase (EC 1.14.18.1) catalyzes the monophenolase and diphenolase reaction associated with vertebrate pigmentation and fruit/vegetable browning. Tyrosinase is an oxygen-dependent, dicopper enzyme that has three states: E_{met} , E_{oxy} , and E_{deoxy} . The diphenolase activity can be carried out by both the met and the oxy states of the enzyme while neither mono- nor diphenolase activity results from the deoxy state. In this study, the oxidative cyclocondensation of 2-aminophenol (OAP) to the corresponding 2-aminophenoxazin-3-one (APX) by mushroom tyrosinase was investigated. Using a combination of various steady- and pre-steady state methodologies, we have investigated the kinetic and chemical mechanism of this reaction. The k_{cat} for OAP is $75 \pm 2 \text{ s}^{-1}$, $K_M^{OAP} = 1.8 \pm 0.2 \text{ mM}$, $K_M^{O_2} = 25 \pm 4 \text{ }\mu\text{M}$ with substrates binding in a steady-state preferred fashion. Stopped flow and global analysis support a model where OAP preferentially binds to the oxy form over the met ($k_7 \gg k_1$). For the met form, His269 and His61 are the proposed bases, while the oxy form uses the copper-peroxide and His61 for the sequential deprotonation of anilinic and phenolic hydrogens. Solvent KIEs show proton transfer to be increasingly rate limiting for k_{cat}/K_M^{OAP} as $[\text{O}_2] \rightarrow 0 \text{ }\mu\text{M}$ (1.38 ± 0.06) decreasing to 0.83 ± 0.03 as $[\text{O}_2] \rightarrow \infty$ reflecting a partially rate limiting $\mu\text{-OH}$ bond cleavage (E_{met}) and formation (E_{oxy}) following protonation in the transition state. The coupling and cyclization reactions of *o*-quinone imine and OAP pass through a phenyliminocyclohexadione intermediate to APX, forming at a rate of $6.91 \pm 0.03 \text{ }\mu\text{M}^{-1}\text{s}^{-1}$ and $2.59\text{E}-2 \pm 5.31\text{E}-4 \text{ s}^{-1}$. Differences in reactivity attributed to the anilinic moiety of OAP with *o*-diphenols are discussed.

© 2015 Elsevier Inc. All rights reserved.

Introduction

Tyrosinase (E.C. 1.14.18.1) is a member of the type-3 copper protein family catalyzing the monophenolase and diphenolase activity on phenolic/anilinic and catechol, 2-aminophenol and 2-aminoaniline substrates, respectively [1–6]. Representative members of the type-3 copper protein family include: catechol oxidase (CO), hemocyanin (Hc) and tyrosinase (Ty) though members have diverse functions. Tyrosinase is associated with pigmentation catalyzing the first step in melanin biosynthesis – a pigment ubiquitously present in all phyla [6]. The structure of mushroom (*Agaricus bisporus*) tyrosinase (abTy) is a tetrameric protein with 2 heavy (H, 392 aa, ~43 kDa) and 2 light (L, 150 aa, ~14 kDa) chains (2.30 Å resolution, 2Y9W) [7,8]. As a derivative of the *ppo3* gene, the fungal enzyme is structurally homologous to other tyrosinases, only

larger with 110 more residues present as loops connecting conserved secondary structural elements. H-subunits of abTy contain 13 α -helices, 8 mostly short β -strands and many loops, similar to known type-3 protein structures including: tyrosinase structures from *Streptomyces castaneoglobisporus* [9] and *Bacillus megaterium* [10,11] as well as *Octopus dolfeini* Hc [12] and *Ipomoea batatas* catechol oxidase [13]. Within the H-subunit, the dicopper binding domain is comprised of four antiparallel helices ($\alpha 3$, $\alpha 4$, and $\alpha 10$, $\alpha 11$) positioned perpendicularly with CuA is coordinated by H61 ($\alpha 3$), H94 ($\alpha 4$) and H85 (loop connecting $\alpha 3$ to $\alpha 4$) and CuB by H259, H263 ($\alpha 10$) and H296 ($\alpha 11$). The structure of the L-subunit in abTy is best described as a β -trefoil fold with 12 antiparallel β -strands assembled in a cylindrical barrel of six 2-stranded sheets [7]. The L-subunit appears to play a structural role in tetramer formation positioned 25 Å away from the active site as H-subunit turnover number is unaffected by its absence.

The di-copper domain in tyrosinase is classified by three distinct geometric and electronic architectures with alternate function

* Corresponding author.

E-mail address: nmcintyre@xula.edu (N.R. McIntyre).

toward substrate oxidation: E_{deoxy} , E_{met} , and E_{oxy} in addition to an inactive mixed valent copper form [14]. The *oxy*-state (E_{oxy}) of tyrosinase has molecular oxygen bound in a side-on $\mu - \eta^2: \eta^2$ geometry linked to the solvent-bridged *met*-state ($\mu\text{-OH}$) and the reduced *deoxy*-state through the reversible exchange of the ligand as oxygen (E_{deoxy}) or peroxide (E_{met}) [15]. The mechanism for tyrosinase-catalyzed phenol (monophenolase) and *o*-diphenol (diphenolase) oxidation has been investigated using steady-state, transient phase and kinetic isotope effects [16–22]. The monophenolase (monooxygenase) activity is catalyzed by tyrosinase in the E_{oxy} form while the *o*-diphenolase (oxidase) activity results from both E_{met} and E_{oxy} forms of the enzyme [19]. Several tyrosinase studies demonstrate that the E_{oxy} form is stable and subsequently reduced to E_{met} with the concomitant oxidation of *o*-diphenol to the corresponding *o*-quinone [23–25]. Evaluation of the abTy *o*-diphenolase reaction mechanism demonstrate tight O_2 binding in addition to an increased second-order rate constant for the *o*-diphenol substrate to preferentially bind with the E_{met} state over the E_{oxy} form of the enzyme [20]. The monophenolase activity of tyrosinase utilizes an electrophilic aromatic substitution (EAS) mechanism for *ortho*-hydroxylation.

Interestingly, tyrosinase and type-3 model complexes lack an observable kinetic isotope effect (KIE) with *ortho*-deuterated monophenol substrates. This suggests that the *ortho*-deprotonation step in this mechanism is either extremely slow or concerted with the oxygen insertion step. The observation of a normal KIE (>1) was revealed upon deuteration of the phenolic hydrogen for both phenol and *o*-diphenol substrates [16,17,26,27]. With proton inventory solvent KIE (sKIE) studies, the mechanism for monophenolase and diphenolase tyrosinase activity support a partially-rate limiting proton transfer in both E_{met} and E_{oxy} forms attributed to nucleophilic attack by the corresponding phenolate ion to copper [16,17].

Structure–function relationships illustrate drastically altered sKIE values based on the para substituent of the substrate. Therein, the fractionation factors (ϕ) decrease as the observed sKIE for k_{cat} increase with each mode of abTy-dependent oxidation. For monophenolase activity, the lowest fractionation factor values and highest sKIE were observed for substrates with an ionic para substituent. For diphenolase activity, the trend is less clear coupling higher fractionation factors with lower sKIE values compared to those reported for the monophenolase reaction. These findings are consistent with a general base catalytic mechanism important to deprotonate substrate phenolic hydrogens that contribute to the stabilization of slightly altered transition state geometries from either the E_{oxy} or E_{met} reaction coordinates [28–34]. The extent of transition state stabilization through altered protonic interactions support the presence of a far different microenvironment for the diphenolase reaction coordinate compared to that observed for monophenolase activity.

The precedence for 2-aminophenol oxidase activity has been previously observed in several copper containing enzymes (laccase [36], tyrosinase [1] and various homologues such as: grIF [37], phenoxazinone synthase [38]) as well as biomimetic complexes ranging from copper through manganese [39]. The oxidation of

2-aminophenols by tyrosinase has been previously studied showing a mechanism similar to catechol compounds [2]. For *o*-aminophenol oxidation, the turnover number is decreased relative to the *o*-diphenol substrates though K_M values does not appear to be dramatically affected by the structural difference [1]. The resulting *o*-quinone imine (Q) undergoes a sequential coupling and cyclization towards the corresponding planar 2-3*H*-aminophenoxazin-3-one (APX) structure passing through several proposed intermediates (Scheme 1) [35,40]. Our current study of 2-aminophenol oxidation by abTy was performed to increase the present body of data contrasting the oxidase mechanism for 2-aminophenol with *o*-diphenol. The role of the phenylamine moiety was studied using a mixture of steady-state and transient phase kinetics, sKIEs, global analysis and molecular modeling studies to characterize multiple aspects of the enzymatic and non-enzymatic reaction coordinate for 2-aminophenol oxidation. Therein, we present experimental evidence supporting a distinct preference for 2-aminophenol oxidation by the E_{oxy} form of abTy (over the more stable E_{met} form) to produce the *o*-quinone imine product which passes through a spectroscopically observed transient phenyliminocyclodione intermediate prior to APX product formation.

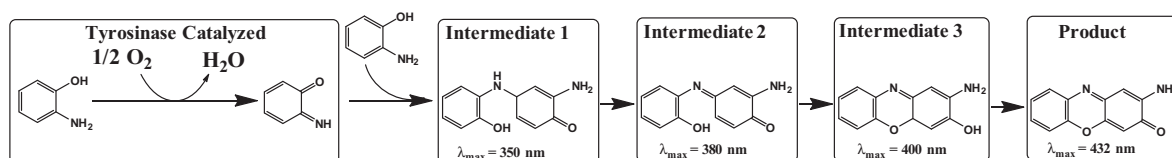
Materials and methods

Reagents

Mushroom tyrosinase (3300 U/mg), 2-aminophenol, L-ascorbic acid, D_2O , mono-, di- and tri-sodium phosphate, DMSO, DMSO- d_6 and purchased from Sigma–Aldrich Co. (St. Louis, MO). HPLC-grade solvents (acetonitrile, methanol, and water) were purchased from Fisher Scientific (Fair Lawn, NJ). Analytical standards were purchased from Sigma–Aldrich Co. (St. Louis, MO). All other experimental reagents were purchased from commercial sources at highest purity grade available and used without additional modification. Commercial enzyme was purified following the procedure of Duckworth and Coleman [41] or the IMAC method [42]. Protein concentration was determined by the bicinchoninic acid assay [43] with bovine serum albumin as standard. Protein purity was assessed by sodium dodecyl sulfate–polyacrylamide gel electrophoresis.

Oxygen electrode

Reactions at 37.0 ± 0.1 °C were initiated by the addition of $\sim 0.10\text{--}0.50$ μM mushroom tyrosinase (4–5 μL) into 2.0 mL of 100 mM sodium phosphate (pH 6.4). Initial velocities were measured at varying concentrations of 2-aminophenol and oxygen. Initial rates were measured by following the tyrosinase-dependent consumption of O_2 using a Yellow Springs Instrument Model 5300 oxygen monitor interfaced with a personal computer using a Dataq Instruments analogue/digital converter (model DI-158RS) interfaced to Microsoft Excel through the Windaq module, modified from McIntyre et al. [44]. Using a Maxtec Low flow oxygen blender, *in situ* $[\text{O}_2]$ was changed by varying the percent mixtures



Scheme 1. Reaction stoichiometry for the tyrosinase catalyzed oxidation of 2-aminophenol to *o*-quinone imine followed by *non-enzymatic* coupling with 2-aminophenol passing through several proposed intermediate structures to give 2-amino-3*H*-phenoxazin-3-one (product). Please note, estimates for the λ_{max} for intermediates were based on previous work by Barry et al. [35].

of oxygen and argon standardized to air-saturated distilled water at 37.0 ± 0.1 °C. Turnover numbers were normalized to controls performed at 8.99 mM 2-aminophenol to account for differences in specific activity between different lots of enzyme. Background O_2 consumption rates were first determined without enzyme and were subtracted from the rate obtained upon tyrosinase addition. Initial rates were determined from the consumption of dissolved oxygen and converted to *o*-quinone imine production or 2-aminophenol consumption using a 2:1 substrate or product to oxygen ratio (Eq. (1)).

$$v_o = -\frac{1}{2} \frac{d[O_2]}{dt} = -2 \frac{d[OAP]}{dt} = 2 \frac{d[Q]}{dt} \quad (1)$$

Initial rate data was then fit to the bi-substrate Michaelis–Menten equation in SigmaPlot 11.2 using the Enzyme Kinetics module (version 1.3)

$$\text{rate} = \frac{k_{\text{cat}}[OAP][O_2]}{K_1^{O_2} K_M^{OAP} + K_M^{O_2} [OAP] + K_M^{OAP} [O_2] + [OAP][O_2]} \quad (2)$$

where k_{cat} is the turnover number (maximal number of OAP and O_2 molecules converted to *o*-quinone imine per tyrosinase active site per second), K_M^{OAP} and $K_M^{O_2}$ are the Michaelis constants for 2-aminophenol (OAP) and molecular oxygen (O_2), respectively, and $K_1^{O_2}$ is the limiting value of $K_M^{O_2}$ when the [OAP] approaches zero. Due to the high degree of error for the $K_M^{O_2}$ parameter using Eq. (2), a replot of $k_{\text{cat}}^{\text{app}}$ versus $[O_2]$ was fit to Eq. (3) to measure the Michaelis constant for $[O_2]$ under pseudo-first order conditions and fit in Kaleidagraph™.

$$\text{rate} = \frac{k_{\text{cat}}^{\text{app}} \times [O_2]}{K_M^{O_2} + [O_2]} \quad (3)$$

Molecular modeling

The initial coordinates of the *A. bisporus* (mushroom) tyrosinase at 2.30 Å resolution were obtained from the Protein Data Bank (<http://www.rcsb.org/pdb/2Y9X>). The structure was prepared for simulation using the protein preparation module of Schrodinger Drug Discovery Suite 2011–2. Water molecules were removed and copper valence was assigned. In the copper binding domains of the active-site, the $\mu - \eta^2: \eta^2$ oxygen bridged structure (E_{oxy}) and η^2 -hydroxyl bridged structures (E_{met}) were created through the manual insertion of the oxygen species followed by minimization. The Coulson charges for the ligands were generated and Glide XP was used to generate the initial poses. The partial atomic charges utilizing electrostatic potential fitting of the protein-bound ligand were calculated using Q-site then re-docked with these updated charges using Glide XP.

Solvent kinetic isotope effects

The dependence of D_2O on the catalytic efficiency of 2-aminophenol oxidation as a function of oxygen tension was performed in a non-competitive fashion following tyrosinase-dependent oxygen consumption. A 10 mM stock of deuterated 2-aminophenol was prepared with 10% DMSO- d_6 in 50 mM sodium phosphate buffer (pH 6.4) dissolved in D_2O , the reaction buffer was 100 mM sodium phosphate buffer (pH 6.4) dissolved in D_2O . Reactions were initiated at 37.0 ± 0.1 °C with 5 μ L of enzyme (0.5 nm), six 2-aminophenol concentrations from 0.90 to 8.99 mM and five oxygen concentrations ranging from 65 to 850 μ M were used, respectively. The k_{cat}/K_M^{OAP} data was determined using standard Michaelis–Menten kinetics (Eq. (4)) and plotted against oxygen tension fitting the data to Eq. (5). The dependence of pH on the k_{cat}/K_M^{OAP} term was performed using the

2-aminophenol concentration range 0.90–8.99 mM under the same conditions listed above over a phosphate buffer pH range of 5.8–8.5. The individual parameters of the k_{cat}/K_M^{OAP} term (k_{cat} and K_M) were determined using Eq. (4) and plotted against pH and fit by a linear regression function.

$$\text{rate} = \frac{k_{\text{cat}} \times [OAP]}{K_M + [OAP]} \quad (4)$$

The $D(k_{\text{cat}}/K_M^{OAP})$ data versus $[O_2]$ was fit to the following exponential curve in Kaleidagraph™.

$$D\left(\frac{k_{\text{cat}}}{K_M^{OAP}}\right)_{\text{observed}} = \left[D\left(\frac{k_{\text{cat}}}{K_M^{OAP}}\right)_{[O_2] \rightarrow 0 \mu\text{M}} - D\left(\frac{k_{\text{cat}}}{K_M^{OAP}}\right)_{[O_2] \rightarrow \infty} \right] e^{-\alpha x [O_2]} + D\left(\frac{k_{\text{cat}}}{K_M^{OAP}}\right)_{[O_2] \rightarrow \infty} \quad (5)$$

where

$$\alpha = \frac{Dk_1 K_D^{O_2}}{k_7 + k_9} + D\left(\frac{k_{\text{cat}}}{K_M^{OAP}}\right)_{[O_2] \rightarrow 0 \mu\text{M}} + 1 \quad (6)$$

Oxy-tyrosinase

The addition of L-ascorbic acid and hydroxylamine to tyrosinase assays prevent substrate oxidation and reduce the E_{met} form of the enzyme to E_{oxy} [45]. Suppression of the UV-vis spectroscopic signal of oxidized 2-aminophenol was followed using an OLIS refurbished Hewlett–Packard 8452 diode array spectrophotometer. The relative rate of 2-aminophenoxazin-3-one (APX) formation at 432 nm was measured versus L-ascorbic acid concentrations intended to perform the *in situ* reduction of the *o*-quinone imine product ranging from 0 to 6 equivalents (Fig. S.1.).

The stability of the E_{oxy} form of abTy was examined by mixing the E_{deoxy} form with an oxygenated buffer in the absence of the 2-aminophenol substrate. Therein, 80 μ M of the reduced enzyme (E_{deoxy}) was prepared anaerobically (5 vacuum-argon gas cycles) with 6-equivalents of hydroxylamine and rapidly mixed with an oxygen saturated buffer. The signal for E_{oxy} was followed at 345 nm ($\epsilon_{345} = 18 \text{ mM}^{-1} \text{ cm}^{-1}$) with a time course collected at 2 ms intervals [24,25]. Consumption of the E_{oxy} signal in the presence of the 2-aminophenol substrate used 20 μ M E_{oxy} was prepared from the reduced enzyme and oxygen gas (*vide supra*) then rapidly mixed with a 1 mM 2-aminophenol solution containing 6 M equivalents of L-ascorbic acid [20].

All rapid-mix studies were performed using a Kintek Mini-Mixer (KinTek Corp., Austin, TX) at 37 ± 0.1 °C with temperature maintained with a Neslab RTE-110 water circulator. Data was collected and processed using an apparatus designed *in-house* with supplies purchased from Ocean Optics (Ocean Optics, St. Petersburg, FL). Specifically, the signal was collected with the SpectraSuite interface using a USB 2000 + XR spectrophotometer and DH-2000 light source linked to the observation cell through Series 74 collimating lenses (200–2000 nm) and solarization resistant fiber optic cables. All curve fitting and kinetic simulation of this data was analyzed with Kaleidagraph™ and Kintek Explorer Professional (KinTek Corp., Austin, TX).

Non-enzymatic formation of 2-aminophenoxazin-3-one

100 μ M tyrosinase was mixed with 1 mM 2-aminophenol under ambient oxygen saturation at 37 ± 0.1 °C.

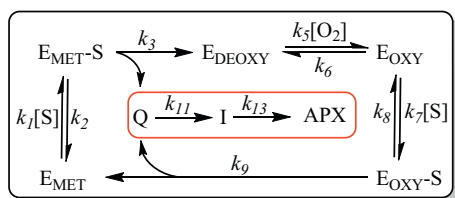
The proposed intermediate was observed at 380 nm and the 2-aminophenoxazin-3-one (APX) product was followed at 432 nm ($\epsilon_{432} = 23.4 \text{ mM}^{-1}\text{cm}^{-1}$). 3-Dimensional analysis of absorbance, time and wavelength were exported from SpectraSuite (Ocean Optics, St. Petersburg, FL.) into the Specfit module of Kintek Explorer Professional (KinTek Corp., Austin, TX) where single value decomposition (SVD) analysis was performed. The spectra was reconstructed from the SVD fits then subtracted from the experimental data to ensure the SVD analysis was statistically relevant. Kinetic constants were constrained by the experimental parameters and calculated using FitSpace to measure the values and show a contour plot.

Kinetic simulation

Kintek Explorer Professional (KinTek Corp., Austin, TX) with the SpecFit module was used for global analysis through direct numerical integration to simulate experimental data [46–48]. The mechanism proposed in Scheme 2 was simulated in two different parts: *catalyzed* and *non-catalyzed* reactions. Each respective path was modeled using the steady- and transient phase data to constrain the minimal kinetic mechanism for the reaction. For the tyrosinase-catalyzed oxidation of 2-aminophenol to the corresponding *o*-quinone imine, a global analysis approach was utilized. Therein, mixtures of pre- and steady-state kinetics were used to evaluate the *catalyzed* minimal kinetic model (Scheme 2). The three states of the enzyme (E_{deoxy} , E_{met} and E_{oxy}) were fit as observables within this model and the experimental data for E_{oxy} was added. The experimental E_{oxy} data was compared to models showing $k_1 \gg k_7$ and $k_1 \ll k_7$ to distinguish the relative ability of E_{met} and E_{oxy} to oxidize 2-aminophenol to *o*-quinone imine, respectively. For the non-enzymatic coupling and cyclization (*non-catalyzed*) reaction of the *o*-quinone imine (Q) to 2-aminophenoxazin-3-one (APX) the time resolved spectra were recalculated using a single value decomposition (SVD) analysis calculated from a matrix-representation. This was the ideal method over global analysis because there were far more wavelengths than species. Using singular values, the statistical relevance of the reconstructed spectra (relative contribution and weights) was compared with experimental values and evaluated through residual analysis. For the *non-catalyzed* reaction, an irreversible two-step kinetic model was used for the formation of APX through a single intermediate. This intermediate represents the accumulation of a transient species associated with early stage coupling steps in the reaction of Q with OAP required to form APX. FitSpace was used to calculate a contour plot for rate constants associated accumulation and decay of this spectroscopically detected intermediate.

HPLC-MS/MS analysis

Lyophilized samples were prepared from 8.99 mM (18 micromoles) of 2-aminophenol oxidized with 750 pmol mushroom tyrosinase in 100 mM sodium phosphate (200 micromoles) buffer



Scheme 2. Minimal kinetic mechanism of the tyrosinase dependent catalytic oxidation of 2-aminophenol (S) to *o*-quinone imine (Q) and its non-enzymatic cyclization to 2-amino-3H-phenoxazin-3-one (APX) passing through an intermediate (I).

(pH 6.4). The reaction was incubated at 37 °C for about 6 h. Prior to HPLC analysis, samples were precipitated by centrifugation at room temperature, and the solvent was evaporated with a stream of nitrogen at 37 °C. The residual solution was applied to 6-mL SUPELCO C₁₈ solid-phase extraction (SPE) columns pretreated with water and methanol. The columns were washed with HPLC-grade water followed by elution with methanol. The effluents were again concentrated by a nitrogen stream at 37 °C to near dryness before reconstitution with methanol to 1 mL volume for HPLC injection. Samples were analyzed on a linear ion trap tandem mass spectrometer (LTQ) interfaced with a Surveyor HPLC system (Thermo-Fisher Scientific, West Palm Beach, FL). Chromatographic separations were achieved by using a Synergi 4u Hydro-RP 80A column (150 × 2.0 mm, 4 μm particle size; Phenomenex, Torrance, CA). Samples were eluted from the analytical column with mobile phase A (water with 0.1% formic acid) and mobile phase B (acetonitrile with 0.1% formic acid) at a flow-rate of 0.2 mL/min over 22 min using a linear gradient of 0–100% B for 13 min; holding at 100% B for 5 min before returning to 0% B.

Results

Product characterization

Tandem LC-MS/MS analysis demonstrates two retention times associated with substrate and product structure (Fig. S.2.). The first retention time of 3.41 min corresponds to a high relative intensity peak (M+1) at 110.09 *m/z* for 2-aminophenol (MW 109.13), tandem MS/MS analysis of this peak gave a fragmentation pattern with peaks at 93.17, 92.13 *m/z* corresponding to the hydroxide loss ($\text{C}_6\text{H}_6\text{N}^+$ and $\text{C}_6\text{H}_5\text{N}^+$) and an 82.16 *m/z* representing phenol rearrangement resulting in an M-28 (CO removal) fragment ($\text{C}_5\text{H}_6\text{N}$). The retention time at 11.60 min shows the highest relative intensity peak (M+1) at 213.06 *m/z* for 2-amino-3H-phenoxazin-3-one (MW 212.06). Tandem MS/MS analysis of the 213.06 *m/z* peak gives two peaks at 185.03 and 186.11 *m/z* corresponding to loss of methylamine ($-\text{CNH}$, 27 *m/z* and $-\text{CNH}_2$, 28 *m/z*).

Steady and transient state kinetics

The steady-state kinetics for the oxidation of 2-aminophenol to the corresponding *o*-quinone imine (Q) was fit to the bi-substrate Michaelis–Menten Eq. (2). Shown in Fig. 1, the k_{cat} is $75 \pm 2 \text{ s}^{-1}$ with a K_M^{OAP} of $1.8 \pm 0.3 \text{ mM}$ with a large error on the $K_M^{\text{O}_2}$ and $K_D^{\text{O}_2}$ values. Replotting the rate of 2-aminophenol oxidation as a function of oxygen concentration under pseudo-first order conditions provides a $K_M^{\text{O}_2}$ value of $25 \pm 4 \text{ μM}$ (Fig. S.3.). Shown in Fig. S.2.A, the double reciprocal plot of 1/rate versus 1/[2-aminophenol] intersects on the abscissa while the 1/rate versus 1/[Oxygen] intersects to the left with a positive y-coordinate, represented as $y = [E_{\text{Total}}]^{-1}((k_6 - k_{\text{cat}})/(k_5 k_{\text{cat}})) = 0.097 \text{ s}$ [20]. A replot of the 1/rate versus 1/[2-aminophenol] slope determined for each oxygen concentration (plotted as 1/[O₂]) crosses the ordinate at a value greater than 0 (Fig. S.4.).

The binding of O₂ to chemically reduced enzyme prepared anaerobically (E_{deoxy}) shows the formation of E_{oxy} observed at 345 nm to be stoichiometric to the initial concentration of the enzyme, activating approximately 92%. Following equilibration, the rate of decay for E_{oxy} was observed to be slow, $6.50 \times 10^{-4} - \text{μM s}^{-1}$ (Fig. S.5.). The E_{oxy} form of tyrosinase was rapidly mixed with 2-aminophenol with L-ascorbic acid for the *in situ* reduction of *o*-quinone imine (Q). Under saturating oxygen conditions, the consumption of the E_{oxy} signal corresponding to $13 \pm 2 \text{ μM}$ enzyme followed a single exponential decay function corresponding to $3.1 \pm 5.6\text{E}-2 \text{ μM}^{-1} \text{ s}^{-1}$ (Fig. 2).

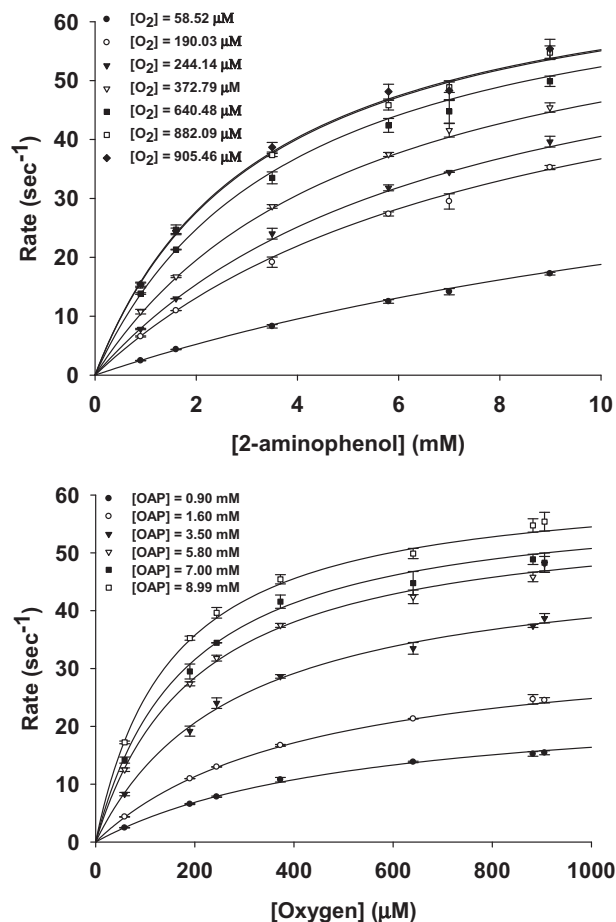


Fig. 1. Steady-state kinetics for the tyrosinase dependent oxidation of 2-aminophenol as a function of oxygen tension. Rates were fit with the bi-substrate Michaelis–Menten equation (Eq. (2)).

The kinetic complexity of the tyrosinase-dependent oxidation of 2-aminophenol to *o*-quinone imine (Q) make direct analysis difficult (see Appendix for distribution equations). Therefore, elementary rate constants for the minimal kinetic mechanism presented in Scheme 2 were determined through a mixture of steady-state and transient phase analysis. Coefficients within the bi-substrate Michaelis–Menten equation are defined according to Scheme 2.

Kinetic simulation using global fitting analysis of the proposed minimal kinetic mechanism (Scheme 2) is shown in Tables 1 and 2. Using E_{met} , E_{deoxy} , and E_{oxy} as ‘observables’ to validate our kinetic model against the experimentally determined rate for E_{oxy} consumption (k_7) to analyze whether 2-aminophenol preferentially reacts with E_{met} or E_{oxy} (Table 2). Rate constants in our model assumed that product release (Q) was equal to k_{cat} representing with k_3 and k_9 while the rate constants k_1 , k_5 , k_6 , k_7 were fixed to the values derived in Table 1 while k_2 and k_8 were each fixed to 0.1 s^{-1} . The values for k_7 were determined through global fitting analysis of the mechanism to be $0.804 \pm 0.041 \mu\text{M}^{-1}\text{s}^{-1}$. According to Fig. 3 (top), $k_1 \ll k_7$ displayed strong correlation between the experimental and theoretical values for E_{oxy} throughout the time course. Validation of this model was performed by reversing the values of k_1 and k_7 ($k_7 \ll k_1$) and comparing the experimental values for E_{oxy} with simulated values where dramatic shift in the theoretical E_{oxy} away from the experimental value was observed (Fig. 3, bottom).

The mechanism for the non-enzymatic coupling of the *o*-quinone imine (Q) product with 2-aminophenol was predicted to pass through several intermediates leading to the APX product

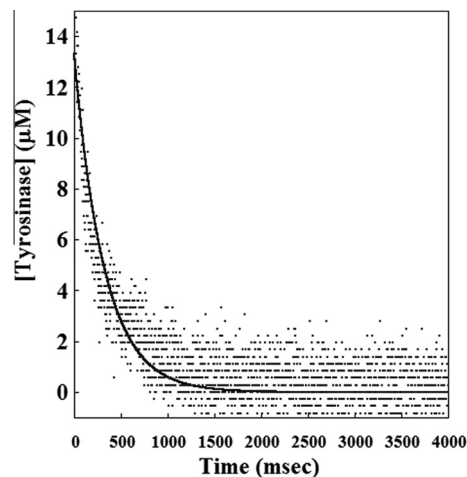


Fig. 2. Stopped-flow analysis of E_{oxy} consumption in the presence of 2-aminophenol. Pre-steady state kinetics were measured at 345 nm upon mixing oxytyrosinase (E_{oxy}) with 1 mM 2-aminophenol with data fit to a single exponential function.

Table 1

Derivation and determination of rate constants from for the 2-aminophenol oxidase activity from steady-state kinetics according to Scheme 2.

$$k_{cat} = k_3 k_9 / (k_3 + k_9)$$

$$K_{1,O_2} K_M^{OAP} = k_3 k_6 k_9 / [k_5 k_7 (k_3 + k_9)] = k_{cat} K_D^{O_2} / k_7$$

$$K_M^{O_2} = k_3 k_9 / [k_5 (k_3 + k_9)] = k_{cat} / k_5$$

$$K_M^{OAP} = [k_3 k_9 (k_1 + k_7)] = [k_{cat} (k_1 + k_7) / k_1 k_7]$$

$$\frac{k_{cat}}{K_M^{OAP}} = k_5 = 3.00 \pm 0.0048 \mu\text{M}^{-1} \text{ s}^{-1}$$

$$\frac{k_{cat}}{K_M^{OAP}} = \frac{k_1 \times k_7}{k_1 \times k_7}$$

If $k_7 \gg k_1$ the 2nd order rate constant for OAP binding to E_{met} becomes

$$\frac{k_{cat}}{K_M^{OAP}} = k_1 = 0.0421 \pm 0.0048 \mu\text{M}^{-1} \text{ s}^{-1}$$

$$K_D^{O_2} = \frac{k_6}{k_5}$$

$$k_6 = K_D^{O_2} \times k_5 = 97 \pm 73 \text{ s}^{-1}$$

Table 2

Steady-state kinetic parameters and rate constants corresponding to the minimal kinetic mechanism representing the best global fit analysis of steady and pre-steady state kinetics of 2-aminophenol (S) oxidation to *o*-quinone imine (Q) and single value decomposition (SVD) analysis of the cyclization of Q and S to form 2-amino-3H-phenoxazin-3-one (APX). Please note that k_2 and k_8 were fixed to 0.1 s^{-1} and that k_{11} and k_{13} were determined using the FitSpace module of Kintek Explorer Professional.

Steady state kinetic parameters		
k_{cat}	75 ± 2	s^{-1}
$K_{M,OAP}$	1.8 ± 0.2	mM
K_{M,O_2}	25 ± 4	μM
K_{D,O_2}	33 ± 24	μM
Rate constants		
k_1	42.1 ± 4.8	$\text{mM}^{-1}\text{s}^{-1}$
k_2	0.1	s^{-1}
k_3	150	s^{-1}
k_5	3000	$\text{mM}^{-1}\text{s}^{-1}$
k_6	97	s^{-1}
k_7	804 ± 41	$\text{mM}^{-1}\text{s}^{-1}$
k_8	0.1	s^{-1}
k_9	150	s^{-1}
k_{11}	6910 ± 31	$\text{mM}^{-1}\text{s}^{-1}$
k_{13}	$2.54\text{E}-2 \pm 5.31\text{E}-4$	s^{-1}

(Scheme 1). Fig. 4 shows time resolved spectra for a transient peak at 380 nm (I) followed by a peak at 432 nm (APX). SVD de-convolution of observable species and spectra reconstruction demonstrate that the residual of the experimental and simulated

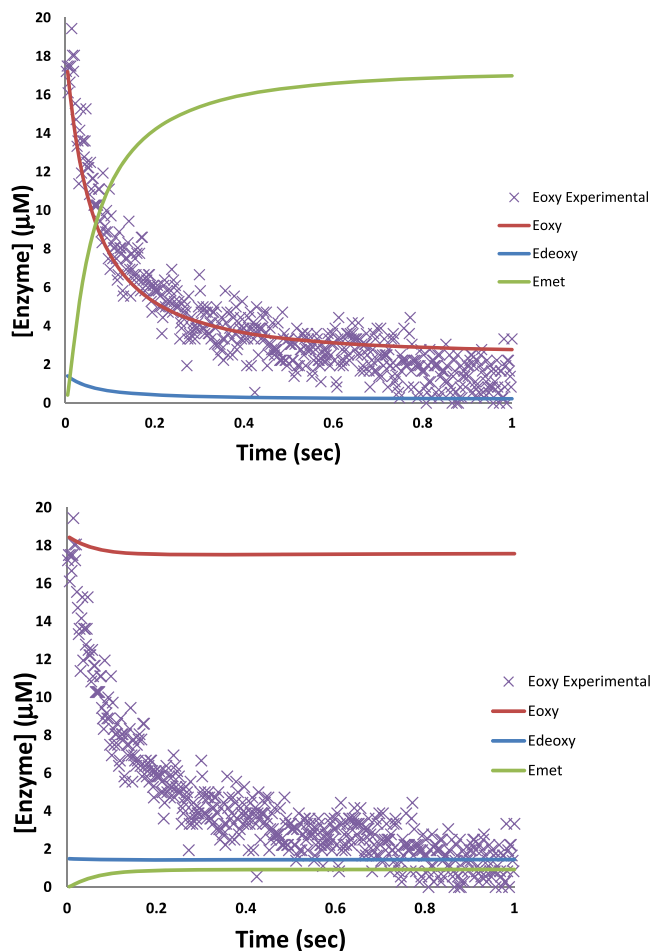


Fig. 3. Model validation correlating simulated data representing the distribution of tyrosinase enzyme states with experimentally derived data for a time course. Each simulation was calculated using kinetic data fit to the global model with $k_7 \ll k_1$ (top) or $k_7 \gg k_1$ (bottom) where the calculated values were switched and compared directly with E_{oxy} values determined experimentally.

spectra are well matched (Fig. S.6.). Analysis of rate constants for the reaction model with global analysis show k_{11} and k_{13} to be $6.91 \pm 0.03 \mu\text{M}^{-1}\text{s}^{-1}$ and $2.59\text{E}-2 \pm 5.31\text{E}-6 \text{ s}^{-1}$ (Table 2) with contour diagram generated through FitSpace showing the data to be well constrained within the model (Fig. S.7.). By correlating the absorbance of APX ($\epsilon_{432} = 23.4 \text{ mM}^{-1}\text{cm}^{-1}$) with the observed intermediate, a $\epsilon_{380} = 7.7 \text{ mM}^{-1}\text{cm}^{-1}$ was determined and the extracted data was fit to a time course that reflected concentration (Fig. S.8.).

The dependence of SKIE on oxygen tension was studied for $k_{\text{cat}}/K_M^{\text{OAP}}$ (Fig. 5). The results clearly demonstrate that proton transfer is increasingly rate limiting to the catalytic efficiency for the tyrosinase-dependent oxidation of OAP as $[\text{O}_2] \rightarrow 0 \text{ mM}$, extrapolating to a value of $D_2\text{O}(k/K) = 1.38 \pm 0.06$. As $[\text{O}_2] \rightarrow \infty$, the reaction displays an inverse solvent kinetic isotope effect, 0.83 ± 0.03 . Pertinent to the SKIE studies, pH versus $k_{\text{cat}}/K_M^{\text{OAP}}$ showed near constant value of $\sim 4 \text{ mM}^{-1}\text{s}^{-1}$ over a broad range (5.7–8.5) (Fig. S.8.).

Molecular modeling

Docking orientation in the E_{met} form shows both 2-aminophenol and catechol to interact with the imidazole side chain of His263 in the CuB binding domain. The distance between N_{ϵ} -His263 and the anilinic hydrogen of 2-aminophenol was 2.26

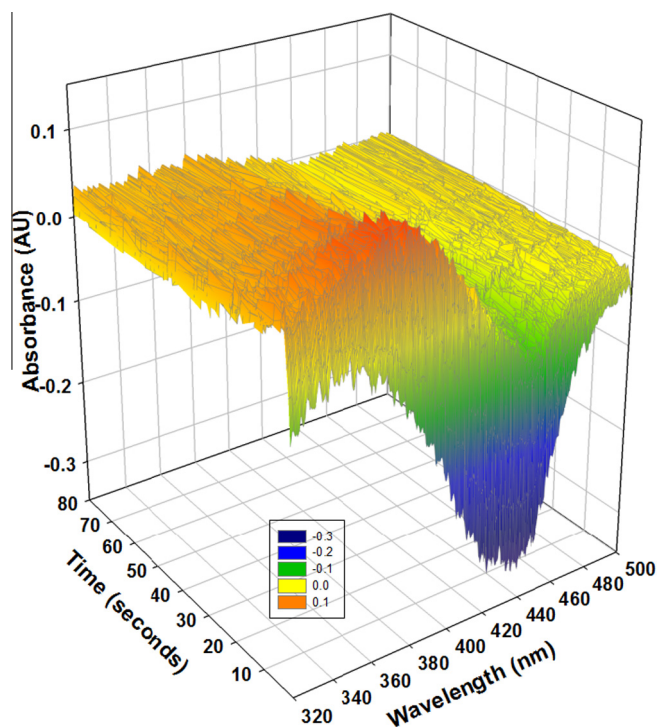


Fig. 4. Time resolved spectra for 2-amino-3H-phenoxazinone (APX) formation from 2-aminophenol and mushroom tyrosinase.

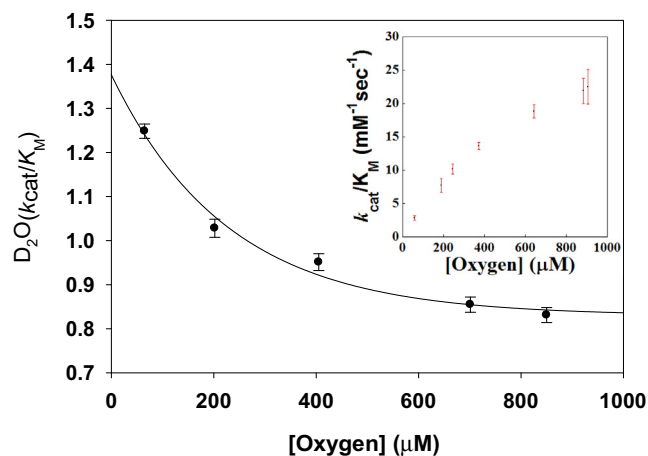


Fig. 5. Solvent kinetic isotope effects on the catalytic efficiency ($k_{\text{cat}}/K_M^{\text{OAP}}$) as a function of oxygen tension and fit to Eq. (5). The inset displays the dependence of ($k_{\text{cat}}/K_M^{\text{OAP}}$) with oxygen concentration.

and 3.71 Å for the corresponding phenolic hydrogen of catechol (Fig. 6). For E_{oxy} the distance of the 2-aminophenol N–H distance to the peroxide was 2.42 and 2.34 Å for the OH group of catechol (Fig. 7). For both E_{met} and E_{oxy} active site architectures, both substrates share nearly superimposable benzene ring stacking with the His296 imidazole moiety and hydrogen bonding with Asn260.

Discussion

Oxygen binds with high affinity to mushroom tyrosinase [49]. Binding of O_2 to abTy is best characterized as a two-electron exchange stabilization of triplet O_2 [50–52]. In the E_{oxy} form, the O_2 is reversibly activated through a peroxide dicopper(II) complex that is highly conserved in type-3 proteins, including Hc and Ty.

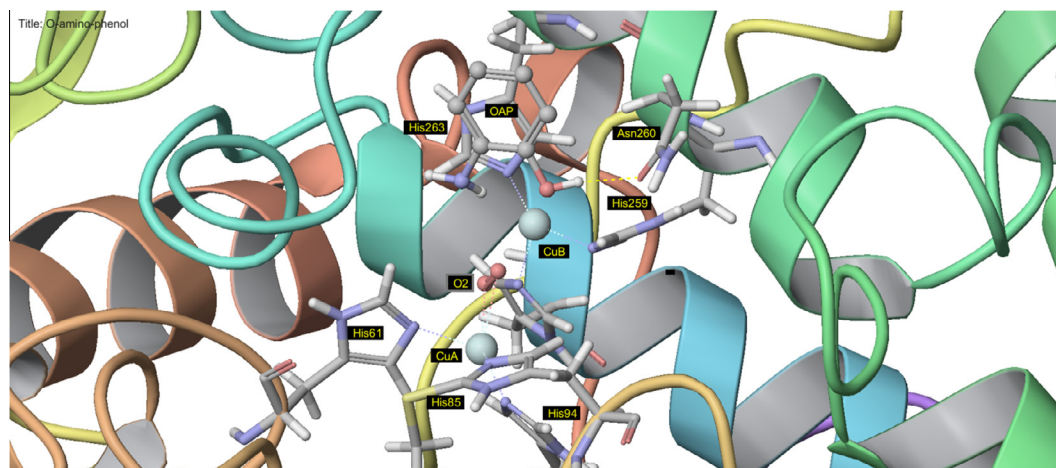


Fig. 6. Binding orientation of 2-aminophenol in the active site of the E_{oxo} form of mushroom tyrosinase. The active site contains copper coordinating histidines (tube), a bridging peroxide for CuA and CuB which hydrogen bonds the amino moiety of 2-aminophenol(OAP). For clarity, catechol was not included but (like E_{met}) shares an indistinguishable binding mode with 2-aminophenol. All other residues that extend beyond the active site are represented by their secondary structural elements.

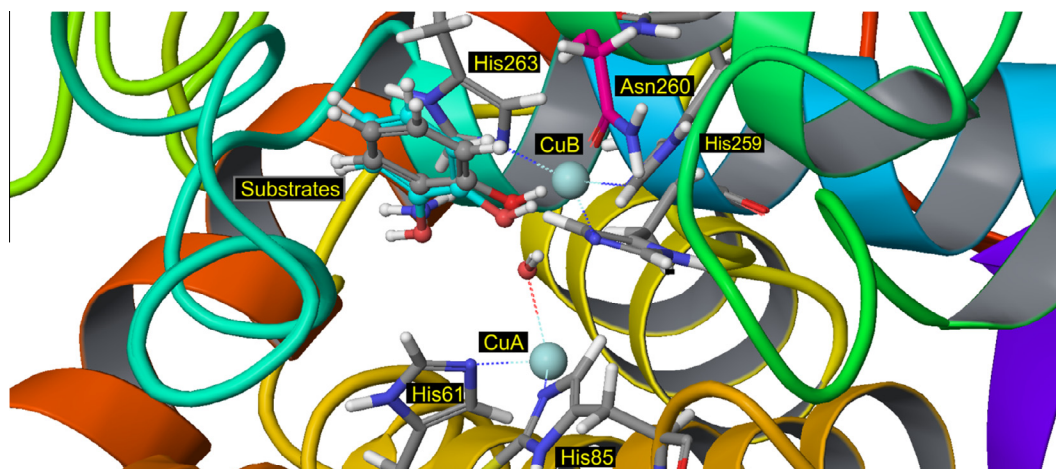
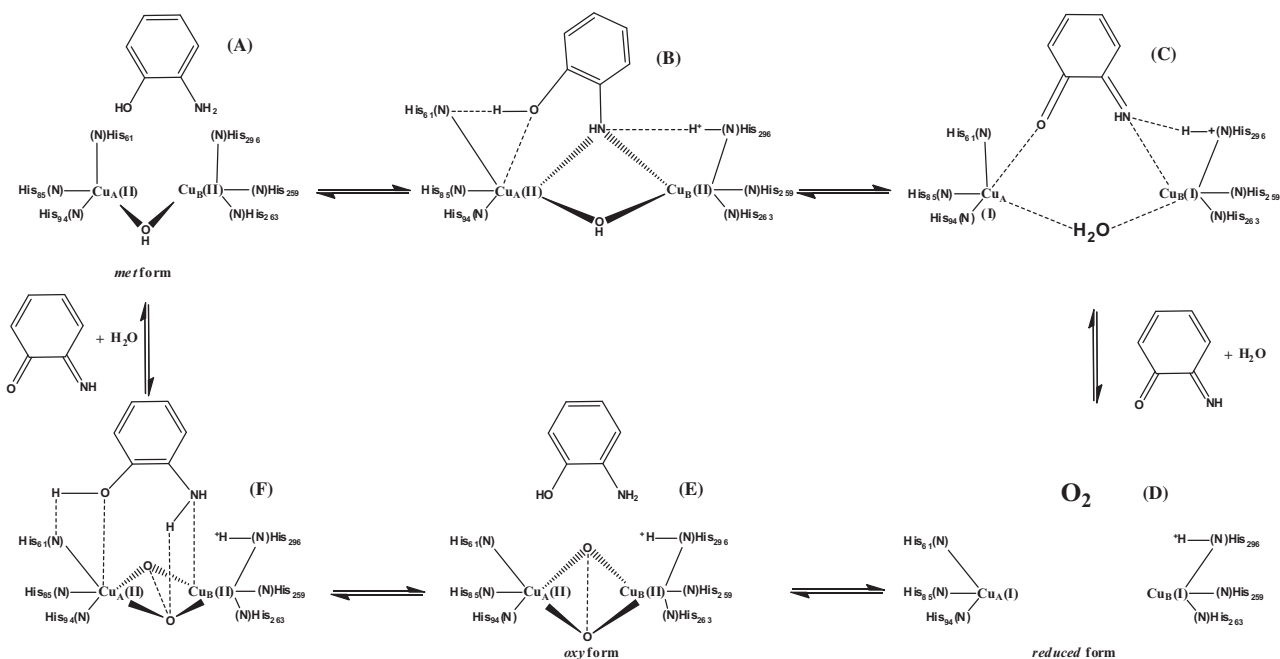


Fig. 7. Homologous binding mode of 2-aminophenol and catechol ('Substrates') in the active site of the E_{met} form of mushroom tyrosinase. Please note, the E_{met} active site contains copper coordinating histidines (tube) with bridging hydroxide (ball and stick) ion for CuA and CuB. Please note the hydrogen bonding between the hydroxyl moiety of each substrate with Asn260. All other residues that extend beyond the active site are represented by their secondary structural elements.

Binding of O_2 to the dicuprous E_{deoxy} state results in filling the π^* HOMO (highest occupied molecular orbital) through two electron reduction to peroxide (O_2^{2-}) to overcome the spin-forbidden triplet state oxygen ($^3\text{O}_2$) containing two unpaired electrons situated in the doubly degenerate π^* orbital. In the E_{oxo} form, the side-on $\mu - \eta^2 : \eta^2$ geometry is responsible for direct orbital overlap (coordination) necessary to produce the intense ligand to metal charge transfer (LMCT) band and is the most favorable orbital overlap for dioxygen reduction to peroxide (E_{oxo}) [53]. The resulting peroxide character of the LMCT is associated with $\text{O}_2^{2-} \pi_{\sigma}^* \rightarrow \text{Cu(II)} (d_{x^2-y^2})$ interactions responsible for significant peroxide character in the LUMO. These π_{σ}^* interactions allow strong σ donation into $d_{x^2-y^2}$ of Cu allowing a π_{σ}^* superexchange pathway to stabilize the singlet state of the Cu_2/O_2 complex and subsequently weaken the O–O bond resembling a bis- μ -oxo complex [54].

The oxidation of 2-aminophenol to o-quinone imine (Q) by abTy was explored using steady-state kinetic analysis (Fig. 1). The similarity in $K_M^{\text{O}_2}$ and $K_D^{\text{O}_2}$ values (25 ± 4 and $33 \pm 24 \mu\text{M}$) using the bi-substrate Michaelis–Menten Eq. (2) suggests an *equilibrium ordered* mechanism for substrate binding, though the replot of the slopes in the $1/\text{rate}$ versus $1/[\text{OAP}]$ plot versus $1/[\text{O}_2]$ clearly show the line does not pass through the origin, supporting that

the difference in $K_M^{\text{O}_2}$ and $K_D^{\text{O}_2}$ values is relevant (Figs. S.3. and S.4.) [55]. With $K_M^{\text{O}_2} < K_D^{\text{O}_2}$, there is synergistic binding of substrates suggesting 2-aminophenol binds tighter to the enzyme in the presence of oxygen to form E_{oxo} . The positive y -coordinate within the x,y intersection in the $1/\text{rate}$ versus $1/[\text{oxygen}]$ (Fig. S.2.A) indicates that the rate of O_2 release is faster than that of Q release ($k_6 > k_{\text{cat}}$) which is further demonstrated through derivation of this rate constant in the Table 1 ($k_6 = 97$ and $k_{\text{cat}} = 75 \text{ s}^{-1}$). Therefore, the binding regime for substrates to the E_{deoxy} form is best described as a *steady-state ordered* mechanism with high error in the $K_D^{\text{O}_2}$ measurement attributed to the tighter binding of the oxygen to the type-3 catalytic center compared with 2-aminophenol [49]. Transient state kinetics following the E_{oxo} form of abTy show the signal for the normally stable E_{oxo} active site architecture to be consumed in single exponential fashion in the presence of 2-aminophenol (Figs. S.5. and 2). The rate for this process (k_7) was determined to be over 15-fold faster than the corresponding rate for the E_{met} (k_1) form of abTy derived from $k_{\text{cat}}/K_M^{\text{OAP}}$ (Table 2). The observation that $k_7 \gg k_1$ supports a model of preferred 2-aminophenol binding to E_{oxo} over E_{met} which is in stark contrast to work pursued with o-diphenol substrates [20]. The rate for k_7 became an experimental



Scheme 3. Proposed mechanism for the tyrosinase dependent oxidation of 2-aminophenol to o-quinone imine.

constraint for the global fitting analysis of the rate constants to validate our proposed model of 2-aminophenol oxidation where $k_7 \gg k_1$ (Table 2). Using global analysis, the best correlation of the experimentally determined values for k_7 was observed for the $k_7 \gg k_1$ simulation supporting our model that 2-aminophenol preferentially binds to the E_{oxy} rather than E_{met} form of abTy (Fig. 3).

An independent measure of the increased reactivity of the *o*-aminophenol substrates for E_{oxy} over E_{met} was further investigated using solvent KIE (sKIE). Previous sKIE values measured at ambient oxygen concentrations show *normal* sKIE values and an accompanying decrease in fractionation factors from reactant to product state ($\phi^R \sim 1 \rightarrow \phi^P < 1$) for both *mono*- and *di*-phenolase activity that results from a single protonic interaction ($n = 1$) [16,17]. The behavior of the same exchangeable position in the abTy reaction coordinate reveal distinct differences from the reactant and product (and presumably the transition) states distinct to the reactions of both E_{met} and E_{oxy} states. Our present sKIE study sought to identify the distribution and relative rate limitation of bridging protonic interactions within the transition state structures for both E_{met} and E_{oxy} forms of the enzyme. To study this effect relative to the abTy enzyme forms present in 2-aminophenol oxidation (E_{met} and E_{oxy}), oxygen tension was varied with data represented as k_{cat}/K_M^{OAP} (Fig. 5). We chose catalytic efficiency (k_{cat}/K_M^{OAP}) over k_{cat} or K_M based on the derivations present in Table 1. Specifically, this term involves both the binding and chemical steps of 2-aminophenol oxidation and is well suited to discriminate proton transfer events between with E_{met} and E_{oxy} forms of abTy. This experimental design requires that the pH-rate profile be independent of the catalytic efficiency. The constant pH-rate profile demonstrates that kinetic data collected in either protiated or deuterated solvent are isolated to the di-coppers involved in catalysis and cannot be attributed to matrix perturbations associated with pH versus pD effects (Fig. S.9.). Our results show a dramatic change in the magnitude of the sKIE as a function of oxygen concentration supporting a model in which the magnitude of the sKIE values are a direct transition state probe of μ -OH

formation and consumption in the E_{met} state. Relative to the transition from E_{oxy} to E_{met} , the extent of μ -OH bond formation is represented as the *inverse* sKIE ($^D(k_{cat}/K_M^{OAP}) < 1$) region of the curve at high $[O_2]$. The increase toward the *normal* sKIE values ($^D(k_{cat}/K_M^{OAP}) > 1$ as $[O_2]$ decreases) demonstrate the partial rate limitation of μ -OH bond cleavage as E_{met} is converted to E_{deoxy} following protonation in the transition state. Compared with 2-aminophenol oxidase sKIE values, the EAS mechanism for phenol hydroxylation by E_{oxy} display the highest sKIE values and support an altered binding mode compared with *o*-diphenol substrates [56–58]. Therefore, the transition from E_{oxy} to E_{met} is rate-limiting for phenol hydroxylation while it serves as a thermodynamic drive for the 2-aminophenol oxidase reaction.

Based on sKIE results from this study and others, a mechanism was postulated to address the unexpected preference of 2-aminophenol for E_{oxy} form of abTy. In Scheme 3, pose (A) has the 2-aminophenol substrate orienting itself with the anilinic group near His296. Structure (C) follows anilinic group de-protonation by His296. Based on crystal structure data for abTy and *B. megaterium* tyrosinase there is precedence for numerous stable conformations and copper mobility present in type-3 dicopper architectures [7,9,59]. Therein, multiple metal ion binding modes for this structure were described through a cooperative model describing high copper ion plasticity controlling reactivity and substrate selectivity of the active site coppers is thought to limit CO to diphenolase activity and Hc to reversible oxygen binding. In support of copper ion plasticity and sampling between different enzyme forms, the reversible oxygen binding with Hc was altered through the addition of a denaturant (SDS) that moved blocking residues opening the active site to the catalytic oxidation of the diphenolic substrate dopamine while CO has copper coordinating histidine residues positioned in a conformationally labile loop regions [60,61]. Based on our molecular modeling studies, the proposed binding orientations for 2-aminophenol and catechol are essentially superimposable with respect to benzene ring positioning near H296 and proximity to the Cu_A–Cu_B binding domains for both E_{met} and E_{oxy} forms of abTy (Figs. 6 and 7). The similarity in

spatial orientation providing a π - π binding interaction with His296 and the benzene ring proposes that any difference in reactivity is solely due to differences in the functional group substitution of aniline for a phenolic moiety within the *o*-diphenol substrate scaffold.

Beginning with the E_{met} form of the enzyme, we propose a mechanism in which the μ -phenylamine of 2-aminophenol coordinates the dicopper domain resulting in a conformational change in the tertiary structure. Similar to reversible O_2 binding in the type-3 proteins, the μ -phenylamine structure would maintain the appropriate superexchange pathway while increasing the hydroxide ion character of the solvent derived μ -OH allowing the capture of a phenolic proton by His61 allowing reduction of the copper domains to E_{deoxy} with concomitant oxidation to the *o*-quinone imine (Q) product (Complex C). The resulting E_{deoxy} form binds molecular oxygen then 2-aminophenol where the bases in this form are the μ - η^2 : η^2 dicopper peroxide for the anilinic roton and His61 for the phenolic proton followed by coordination to the copper centers. The resulting $2e^-$, $2H^+$ redox process yields the second *o*-quinone imine and water with His61 deprotonated to give the characteristic μ -OH of E_{met} (Complexes E and F).

From a combination of kinetic and molecular modeling coupled with solvent kinetic isotope effects, it appears that the E_{met} form has a greater degree of conformational sampling allowing stable quasi-productive binding modes to occur. The μ -phenylamine (complex B) is one postulated intermediate that could cause the reduction of the μ -OH of E_{met} to become slow or rate-limiting to the global catalytic model (Scheme 2). Additional support for conformational mobility in the abTy active site is found by correlating secondary structural elements of the protein with ligand and binding pocket surfaces (Figs. 8 and 9). With respect to 2-aminophenol binding modes in both E_{met} and E_{oxy} , the anilinic moiety is buried in the surface accessible active-site. With a similar interaction with His296 for each enzyme form, the resulting loop extending from the $\alpha 11$ helix defines a significant portion of the substrate binding face. Following proton transfer, subsequent electronic changes in the active site would be expected to sufficiently affect the loop conformation allowing the phenolic group to position near the CuA domain for deprotonation with H61.

Following release of the *o*-quinone imine product, tandem coupling and cyclization of *o*-quinone imine (Q) with 2-aminophenol (OAP) to forms the isolated product 2-amino-3*H*-phenoxazin-3-one (APX) (Figs. S.2. and 4). Previous work on melanin carried out by Riley [62] and dopamine *o*-quinone cyclization [63] explored intramolecular cyclization for compounds biologically relevant to melanogenesis. Based on proposed intermediates and projected λ_{max} values, the spectroscopic signals observed at 380 and 432 nm corresponding to *intermediate 2* and *product* in the nucleophilic intermolecular conjugate addition pathway for APX formation (Scheme 1). Using SVD, the rate of coupling is much faster than the corresponding cyclization ($6.91 \pm 0.3 \mu\text{M}^{-1}\text{s}^{-1}$ and $2.59 \pm 5.31\text{E}-4 \text{s}^{-1}$) passing through a phenyliminocyclohexadione intermediate (Table 2). Using the sequential model proposed in Scheme 1, the extracted data suggest the short lived *o*-quinone imine (Q) enzymatic product undergoes a Michael-type addition with 2-aminophenol resulting in an observed phenyliminocyclohexadione intermediate that cyclizes to the APX product (Fig. 4).

In conclusion, this study shows the oxidative cyclocondensation of 2-aminophenol to undergo an abTy dependent oxidation to its corresponding *o*-quinone imine releasing a water molecule from both E_{met} and E_{oxy} followed by several conjugate addition intermediates leading to the eventual 2-amino-3*H*-phenoxazin-3-one (APX) product (Scheme 3). Within this reaction, the abTy-dependent oxidation of 2-aminophenol was preferentially carried out by the E_{oxy} rather than E_{met} forms of the enzyme. We suggest the additional stabilization of the E_{met} form by the anilinic group of 2-aminophenol relative to *o*-diphenol substrates as an explanation for the difference in reactivity (Scheme 3). The sKIE studies support this model as the rate limitation for proton transfer is greatest with the E_{met} form and lowest (inverse) with E_{oxy} . This suggests that μ -OH formation (E_{oxy} to E_{met}) is favorable compared the rate limiting transition of E_{met} to E_{deoxy} likely caused by the formation of a quasi-stable conformation of the E_{met} containing a μ -phenylamine bridge between CuA and CuB that mimics the bis- μ -oxo dicopper geometry observed in the E_{oxy} form of abTy. Overall, the present study characterized distinct mechanistic differences in the conventional mechanism between *o*-diphenolase and 2-aminophenol oxidase with abTy and followed the

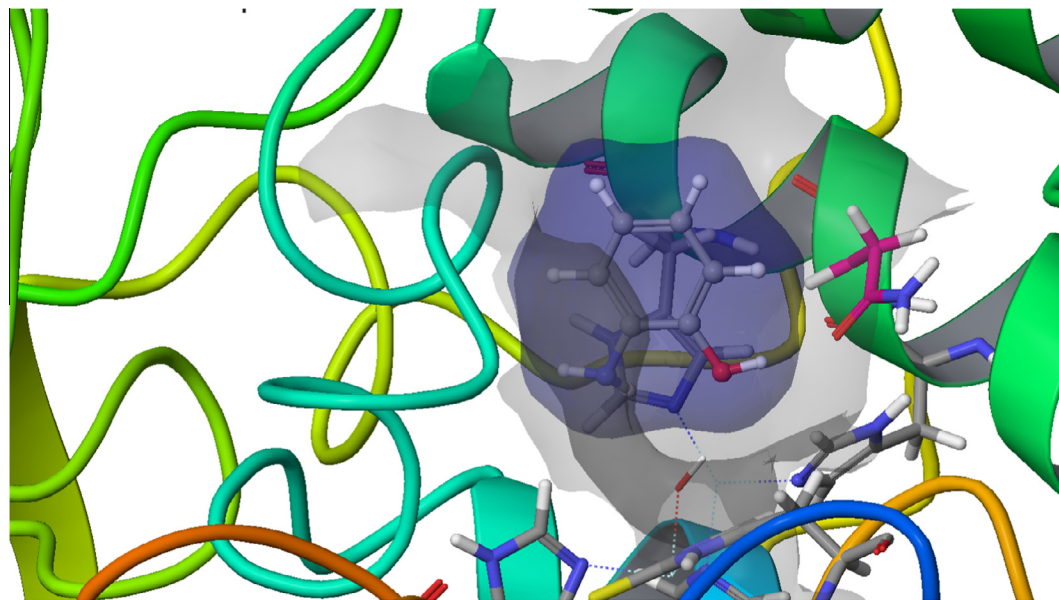


Fig. 8. Representation of the ligand and active site binding surface for 2-aminophenol and the E_{met} form of mushroom tyrosinase. Please note, 2-aminophenol is shown in blue, the binding pocket is covered with a gray with the loop (teal) extending from the $\alpha 11$ -helix (green). (For interpretation of the references to color in this figure legend, the reader is referred to the web version of this article.)

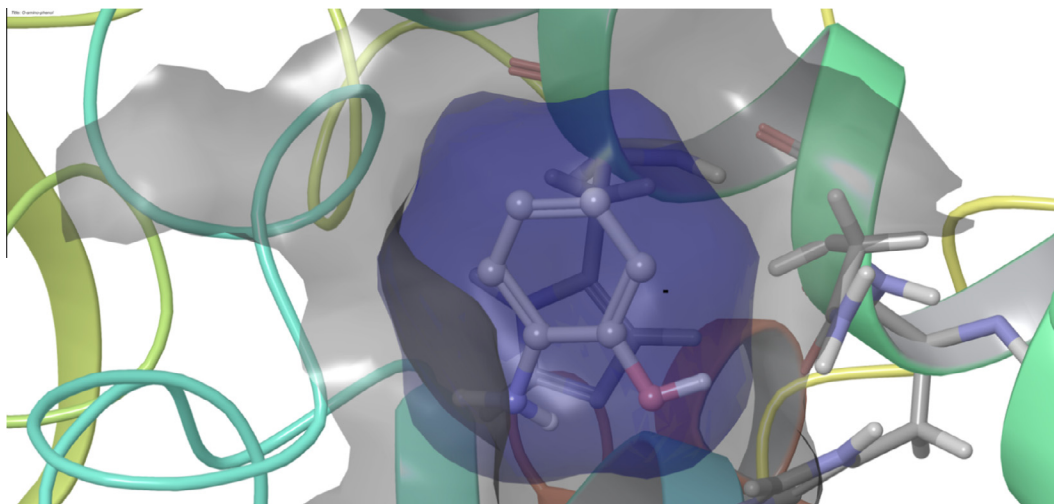


Fig. 9. Binding orientation of 2-aminophenol in the CuB domain of E_{oxo} form of mushroom tyrosinase. Please note, 2-aminophenol is shown in blue, the binding pocket is covered with a gray showing the loop (teal) extending from the $\alpha 11$ -helix (green). (For interpretation of the references to color in this figure legend, the reader is referred to the web version of this article.)

non-enzymatic cyclization through a previously undetected intermediate leading to the APX product.

Acknowledgments

Neil R. McIntyre would like to acknowledge support from NIH-1SC3GM112558-01, NIH-RCMI Grant 2G12MD007595-06, Louisiana Cancer Research Consortium (LCRC), NSF-Louis Stokes Alliance for Minority Participation (JM), Center for Undergraduate Research (CUR)(JS), Louisiana Board of Regents Research Commercialization and Education Enhancement Program (RCEEP)(GM), Department of Chemistry Work/Study. Edward W. Lowe, Jr. acknowledges NSF support through the CI-TraCS fellowship (OCI-1122919). Guangdi Wang would like to acknowledge support from Department of Defense grant W81XWH-04-1-0557, Office of Naval Research Grant N00014-99-1-0763, and LCRC. We would also like to acknowledge the insightful recommendations of Dr. Larry Byers (Tulane) during the preparation of this manuscript.

Appendix A

Distribution Equations

$$\frac{E_{\text{met}}}{E_T} = k_2 k_6 k_8 + k_3 k_5 k_7 k_9 [\text{O}_2][\text{S}] + k_2 k_5 k_7 k_9 [\text{O}_2][\text{S}] + k_2 k_7 k_9 [\text{S}] + k_2 k_6 k_9 / \Delta$$

$$\frac{dQ}{dt} = \frac{k_1 k_5 k_7 k_9 [\text{O}_2][\text{S}]^2 + k_1 k_7 k_9 [\text{O}_2][\text{S}] + k_1 k_6 k_9 [\text{S}] + k_9 k_1 k_3 k_5 k_7 [\text{O}_2][\text{S}]^2 + k_3 k_5 k_7 [\text{O}_2][\text{S}]}{k_3 k_5 k_7 k_9 [\text{O}_2][\text{S}] + k_1 k_5 k_7 k_9 [\text{O}_2][\text{S}]^2 + k_1 k_7 k_9 [\text{O}_2][\text{S}] + k_1 k_6 k_9 [\text{S}] + k_1 k_3 k_7 k_9 [\text{S}]^2 + k_1 k_3 k_6 k_9 [\text{S}] + k_1 k_3 k_5 k_9 [\text{O}_2][\text{S}] + k_1 k_3 k_5 k_7 [\text{O}_2][\text{S}]^2 + k_3 k_5 k_7 [\text{O}_2][\text{S}]}$$

$$\frac{E_{\text{met}} - S}{E_T} = k_1 k_6 k_8 [\text{S}] + k_6 k_8 + k_1 k_5 k_7 k_9 [\text{O}_2][\text{S}]^2 + k_1 k_7 k_9 [\text{O}_2][\text{S}] + k_1 k_6 k_9 [\text{S}] / \Delta$$

$$\frac{E_{\text{deoxy}}}{E_T} = k_1 k_3 k_6 k_8 [\text{S}] + k_3 k_6 k_8 + k_2 k_6 k_8 + k_1 k_3 k_7 k_9 [\text{S}]^2 + k_1 k_3 k_6 k_9 [\text{S}] / \Delta$$

$$\frac{E_{\text{oxo}}}{E_T} = k_1 k_3 k_5 k_8 [\text{O}_2][\text{S}] + k_3 k_5 k_8 [\text{O}_2] + k_2 k_5 k_8 [\text{O}_2] + k_2 k_8 + k_1 k_3 k_5 k_9 [\text{O}_2][\text{S}] / \Delta$$

$$\frac{E_{\text{oxo}} - S}{E_T} = k_1 k_3 k_5 k_7 [\text{O}_2][\text{S}]^2 + k_3 k_5 k_7 [\text{O}_2][\text{S}] + k_2 k_5 k_7 [\text{O}_2][\text{S}] + k_2 k_7 [\text{S}] + k_2 k_6 / \Delta$$

Please note the E_T is total enzyme and represents the sum of all distribution equations for each enzyme form.

Rate of product formation:

$$\frac{dQ}{dt} = k_3 [E_{\text{met}} - S] + k_9 [E_{\text{oxo}} - S]$$

$$\begin{aligned} dQ/dt = & (k_3 k_1 k_6 k_8 [\text{S}] + k_6 k_8 + k_1 k_5 k_7 k_9 [\text{O}_2][\text{S}]^2 + k_1 k_7 k_9 [\text{O}_2][\text{S}] \\ & + k_1 k_6 k_9 [\text{S}] + k_9 k_1 k_3 k_5 k_7 [\text{O}_2][\text{S}]^2 + k_3 k_5 k_7 [\text{O}_2][\text{S}] \\ & + k_2 k_5 k_7 [\text{O}_2][\text{S}] + k_2 k_7 [\text{S}] + k_2 k_6) / (k_2 k_6 k_8 + k_3 k_5 k_7 k_9 [\text{O}_2][\text{S}] \\ & + k_2 k_5 k_7 k_9 [\text{O}_2][\text{S}] + k_2 k_7 k_9 [\text{S}] + k_2 k_6 k_9 + k_1 k_6 k_8 [\text{S}] + k_6 k_8 \\ & + k_1 k_5 k_7 k_9 [\text{O}_2][\text{S}]^2 + k_1 k_7 k_9 [\text{O}_2][\text{S}] + k_1 k_6 k_9 [\text{S}] \\ & + k_1 k_3 k_6 k_8 [\text{S}] + k_3 k_6 k_8 + k_2 k_6 k_8 + k_1 k_3 k_7 k_9 [\text{S}]^2 \\ & + k_1 k_3 k_6 k_9 [\text{S}] + k_1 k_3 k_5 k_8 [\text{O}_2][\text{S}] + k_3 k_5 k_8 [\text{O}_2] + k_2 k_5 k_8 [\text{O}_2] \\ & + k_2 k_8 + k_1 k_3 k_5 k_9 [\text{O}_2][\text{S}] + k_1 k_3 k_5 k_7 [\text{O}_2][\text{S}]^2 + k_3 k_5 k_7 [\text{O}_2][\text{S}] \\ & + k_2 k_5 k_7 [\text{O}_2][\text{S}] + k_2 k_7 [\text{S}] + k_2 k_6) \end{aligned}$$

If $k_3 \gg k_2$ and $k_9 \gg k_8$

Appendix B. Supplementary data

Supplementary data associated with this article can be found, in the online version, at <http://dx.doi.org/10.1016/j.abb.2015.04.007>.

References

- [1] O. Toussaint, K. Lerch, *Biochemistry* 26 (1987) 8567–8571.
- [2] J.L. Munoz-Munoz, F. Garcia-Molina, P.A. Garcia-Ruiz, R. Varon, J. Tudela, J.N. Rodriguez-Lopez, F. Garcia-Canovas, *Biochim. Biophys. Acta* 2011 (1814) 1974–1983.
- [3] C.I. Wright, H.S. Mason, *J. Biol. Chem.* 165 (1946) 45–53.
- [4] H.S. Mason, *J. Biol. Chem.* 172 (1948) 83–99.
- [5] H.S. Mason, *J. Biol. Chem.* 181 (1949) 803–812.
- [6] A. Sanchez-Ferrer, J.N. Rodriguez-Lopez, F. Garcia-Canovas, F. Garcia-Carmona, *Biochim. Biophys. Acta* 1247 (1995) 1–11.
- [7] W.T. Ismaya, H.J. Rozeboom, A. Weijn, J.J. Mes, F. Fusetti, H.J. Wichers, B.W. Dijkstra, *Biochemistry* 50 (2011) 5477–5486.
- [8] W.T. Ismaya, H.J. Rozeboom, M. Schurink, C.G. Boeriu, H. Wichers, B.W. Dijkstra, *Acta Crystallogr., Sect. F: Struct. Biol. Cryst. Commun.* 67 (2011) 575–578.
- [9] Y. Matoba, T. Kumagai, A. Yamamoto, H. Yoshitsu, M. Sugiyama, *J. Biol. Chem.* 281 (2006) 8981–8990.
- [10] M. Sendovski, M. Kanteef, V. Shuster Ben-Yosef, N. Adir, A. Fishman, *Acta Crystallogr. Sect. F Struct. Biol. Cryst. Commun.* 66 (2010) 1101–1103.
- [11] M. Sendovski, M. Kanteef, V.S. Ben-Yosef, N. Adir, A. Fishman, *J. Mol. Biol.* 405 (2011) 227–237.
- [12] M.E. Cuff, K.I. Miller, K.E. van Holde, W.A. Hendrickson, *J. Mol. Biol.* 278 (1998) 855–870.
- [13] T. Klabunde, C. Eicken, J.C. Sacchettini, B. Krebs, *Nat. Struct. Biol.* 5 (1998) 1084–1090.
- [14] C.A. Ramsden, P.A. Riley, *Bioorg. Med. Chem.* 22 (2014) 2388–2395.
- [15] P. Chen, E.I. Solomon, *Proc. Natl. Acad. Sci. USA* 101 (2004) 13105–13110.
- [16] L.G. Fenoll, M.J. Penalver, J.N. Rodriguez-Lopez, P.A. Garcia-Ruiz, F. Garcia-Canovas, J. Tudela, *Biochem. J.* 380 (2004) 643–650.
- [17] M.J. Penalver, J.N. Rodriguez-Lopez, P.A. Garcia-Ruiz, F. Garcia-Canovas, J. Tudela, *Biochim. Biophys. Acta* 1650 (2003) 128–135.
- [18] M.J. Penalver, A.N. Hiner, J.N. Rodriguez-Lopez, F. Garcia-Canovas, J. Tudela, *Biochim. Biophys. Acta* 1597 (2002) 140–148.
- [19] L.G. Fenoll, J.N. Rodriguez-Lopez, F. Garcia-Sevilla, P.A. Garcia-Ruiz, R. Varon, F. Garcia-Canovas, J. Tudela, *Biochim. Biophys. Acta* 1548 (2001) 1–22.
- [20] J.N. Rodriguez-Lopez, L.G. Fenoll, P.A. Garcia-Ruiz, R. Varon, J. Tudela, R.N. Thorneley, F. Garcia-Canovas, *Biochemistry* 39 (2000) 10497–10506.
- [21] J.L. Munoz-Munoz, M. Garcia-Molina Mdel, F. Garcia-Molina, P.A. Garcia-Ruiz, F. Garcia-Sevilla, J.N. Rodriguez-Lopez, F. Garcia-Canovas, *IUBMB life* 65 (2013) 793–799.
- [22] J.L. Munoz-Munoz, F. Garcia-Molina, R. Varon, J. Tudela, F. Garcia-Canovas, J.N. Rodriguez-Lopez, *Acta Biochim. Polonica* 58 (2011) 303–311.
- [23] M.P. Jackman, M. Huber, A. Hajnal, K. Lerch, *Biochem. J.* 282 (Pt 3) (1992) 915–918.
- [24] R.L. Jolley Jr., L.H. Evans, N. Makino, H.S. Mason, *J. Biol. Chem.* 249 (1974) 335–345.
- [25] N. Makino, H.S. Mason, *J. Biol. Chem.* 248 (1973) 5731–5735.
- [26] T. Osako, K. Ohkubo, M. Taki, Y. Tachi, S. Fukuzumi, S. Itoh, *J. Am. Chem. Soc.* 125 (2003) 11027–11033.
- [27] T. Matsumoto, H. Furutachi, M. Kobino, M. Tomii, S. Nagatomo, T. Tosha, T. Osako, S. Fujinami, S. Itoh, T. Kitagawa, M. Suzuki, *J. Am. Chem. Soc.* 128 (2006) 3874–3875.
- [28] D.M. Quinn, L.D. Sutton, in: P.F. Cook (Ed.), *Enzyme Mechanisms from Isotope Effects*, CRC Press, Boca Raton, FL, 1991, pp. 73–126.
- [29] A.J. Kresge, R.A. More O'Ferrall, M.F. Powell, in: E. Buncl, C.C. Lee (Eds.), *Isotopes in Organic Chemistry*, vol. 7, Elsevier, Amsterdam, 1987, p. 177.
- [30] F.J. Alvarez, R.L. Schowen, in: E. Buncl, C.C. Lee (Eds.), *Isotopes in Organic Chemistry*, Elsevier, Amsterdam, 1987, pp. 1–60.
- [31] K.S. Venkatasubban, R.L. Schowen, *Crit. Rev. Biochem.* 17 (1984) 1–44.
- [32] K.B.J. Schowen, R.L. Schowen, *Methods Enzymol.* 87 (1982) 551–606.
- [33] K.B.J. Schowen, in: R.D. Gandour, R.L. Schowen (Eds.), *Transition State of Biochemical Processes*, Plenum, New York, 1978, pp. 225–283.
- [34] R.L. Schowen, in: W.W. Cleland, M.H. O'Leary, D.B. Northrop (Eds.), *Isotope Effects on Enzyme-Catalyzed Reactions*, University Park Press, Baltimore, MD, 1977, pp. 64–99.
- [35] C.E. Barry 3rd, P.G. Nayar, T.P. Begley, *Biochemistry* 28 (1989) 6323–6333.
- [36] F. Bruyneel, O. Payen, A. Rescigno, B. Tinant, J. Marchand-Brynaert, *Chemistry* 15 (2009) 8283–8295.
- [37] H. Suzuki, Y. Furusho, T. Higashi, Y. Ohnishi, S. Horinouchi, *J. Biol. Chem.* 281 (2006) 824–833.
- [38] A.W. Smith, A. Camara-Artigas, M. Wang, J.P. Allen, W.A. Francisco, *Biochemistry* 45 (2006) 4378–4387.
- [39] J. Kaizer, G. Barath, R. Csonka, G. Speier, L. Korecz, A. Rockenbauer, L. Parkanyi, *J. Inorg. Biochem.* 102 (2008) 773–780.
- [40] J.C. Freeman, P.G. Nayar, T.P. Begley, J.J. Villafranca, *Biochemistry* 32 (1993) 4826–4830.
- [41] H.W. Duckworth, J.E. Coleman, *J. Biol. Chem.* 245 (1970) 1613–1625.
- [42] A. Powell, N. Siu, J.K. Inlow, W.H. Flurkey, *J. Chem.* 1 (2007) 1–13.
- [43] P.K. Smith, R.I. Krohn, G.T. Hermanson, A.K. Mallia, F.H. Gartner, M.D. Provenzano, E.K. Fujimoto, N.M. Goeke, B.J. Olson, D.C. Klenk, *Anal. Biochem.* 150 (1985) 76–85.
- [44] N.R. McIntyre, E.W. Lowe Jr., G.H. Chew, T.C. Owen, D.J. Merkler, *FEBS Lett.* 580 (2006) 521–532.
- [45] D.C. Goodwin, I. Yamazaki, S.D. Aust, T.A. Grover, *Anal. Biochem.* 231 (1995) 333–338.
- [46] K.A. Johnson, *Methods Enzymol.* 467 (2009) 601–626.
- [47] K.A. Johnson, Z.B. Simpson, T. Blom, *Anal. Biochem.* 387 (2009) 30–41.
- [48] K.A. Johnson, Z.B. Simpson, T. Blom, *Anal. Biochem.* 387 (2009) 20–29.
- [49] J.N. Rodriguez-Lopez, J.R. Ros, R. Varon, F. Garcia-Canovas, *Biochem. J.* 293 (Pt 3) (1993) 859–866.
- [50] E.I. Solomon, J.W. Ginsbach, D.E. Heppner, M.T. Kieber-Emmons, C.H. Kjaergaard, P.J. Smeets, L. Tian, J.S. Woertink, *Faraday Discussions* 148 (2011) 11–39, discussion 97–108.
- [51] E.I. Solomon, D.E. Heppner, E.M. Johnston, J.W. Ginsbach, J. Cirera, M. Qayyum, M.T. Kieber-Emmons, C.H. Kjaergaard, R.G. Hadt, L. Tian, *Chem. Rev.* 114 (2014) 3659–3853.
- [52] J. Shearer, C.X. Zhang, L.N. Zakharov, A.L. Rheingold, K.D. Karlin, *J. Am. Chem. Soc.* 127 (2005) 5469–5483.
- [53] R.H. Holm, P. Kennepohl, E.I. Solomon, *Chem. Rev.* 96 (1996) 2239–2314.
- [54] M.T. Kieber-Emmons, J.W. Ginsbach, P.K. Wick, H.R. Lucas, M.E. Helton, B. Lucchese, M. Suzuki, A.D. Zuberbuhler, K.D. Karlin, E.I. Solomon, *Angew. Chem. Int. Ed. Engl.* 53 (2014) 4935–4939.
- [55] W.W. Cleland, *Methods Enzymol.* 63 (1979) 103–138.
- [56] F.G. Molina, J.L. Munoz, R. Varon, J.N. Lopez, F.G. Canovas, J. Tudela, *Int. J. Biochem. Cell Biol.* 39 (2007) 238–252.
- [57] S. Naish-Byfield, P.A. Riley, *Pigment Cell Res.* 11 (1998) 127–133.
- [58] C. Olivares, F. Solano, *Pigment Cell Melanoma Res.* 22 (2009) 750–760.
- [59] M. Sendovski, M. Kanteef, V.S. Ben-Yosef, N. Adir, A. Fishman, *J. Mol. Biol.* 405 (2011) 227–237.
- [60] Y. Cong, Q. Zhang, D. Woolford, T. Schweikardt, H. Khant, M. Dougherty, S.J. Ludtke, W. Chiu, H. Decker, *Structure* 17 (2009) 749–758.
- [61] S. Baird, S.M. Kelly, N.C. Price, E. Jaenicke, C. Meesters, D. Nillius, H. Decker, J. Nairn, *Biochim. Biophys. Acta* 1774 (2007) 1380–1394.
- [62] E.J. Land, C.A. Ramsden, P.A. Riley, *Tetrahedron Lett.* 62 (2006) 4884–4891.
- [63] J. Borovansky, R. Edge, E.J. Land, S. Navaratnam, S. Pavel, C.A. Ramsden, P.A. Riley, N.P. Smit, *Pigment Cell Res.* 19 (2006) 170–178.